Appl. Phys. B (2014) 115:443–449
DOI 10.1007/s00340-013-5623-y

Applied Physics B
Lasers and Optics

Seven-photon ultraviolet upconversion emission of Er^{3+} induced by 1,540-nm laser excitation

J. Zheng · X. F. Wang · W. Y. He · Y. Y. Bu · X. H. Yan

Received: 20 March 2013 / Accepted: 19 August 2013 / Published online: 11 September 2013

Abstract The multi-photon ultraviolet upconversion emission properties and synergistic effect are investigated in $BaSr_2Y_6O_{12}:Er^{3+}$ phosphor. The deep-ultraviolet emissions centered at 274, 297 and 324-nm are observed under the 1,540-nm excitation, which results from a seven-, six- and six-photon upconversion process, respectively. A synergistic effect is found, which shows that the red emission intensity under 351- and 1,540-nm dual excitation is 4.7 % time stronger than the sum of red emission intensities under the 351 and 1,540-nm single excitation. This phenomenon is attributed to the $^4I_{13/2}$ and $^4I_{11/2}$ levels of Er^{3+} from non-radiative transition process under the 351-nm excitation are excited again to $^4F_{9/2}$ level by absorbing 1,540-nm photon in the 351- and 1,540-nm dual-excitation process.

1 Introduction

In recent years, the upconversion luminescent properties research has been dominated by the conversion of infrared to visible region [1–3]. While the ultraviolet upconversion emission under 1,540-nm excitation is still greatly restricted, populating the high-energy states needs a multi-photon upconversion process. In the previous reports, the deep-ultraviolet upconversion emissions of Gd^{3+} and Nd^{3+} were detected under the excitation of near-infrared or visible laser [4–7], and the ultraviolet upconversion emission in the region of 270–330 nm from Er^{3+} ions which was sensitized by Yb^{3+}/Gd^{3+} in fluoride material hosts under 1,560-nm excitation has also been reported. These high-lying excited levels were populated through excited state absorption (ESA) and complex energy transition (ET) processes [8, 9].

Among the rare-earth ions, trivalent erbium ions (Er^{3+}) provide several long-lived intermediate levels as well as metastable high energy levels, and the energy gap between the ground level $^4I_{15/2}$ and the first excited level $^4I_{13/2}$ is 6,400 cm^{-1}, which matches well with the absorption of 1,540-nm photon [8, 9]. Also, the wavelengths around 1,540 nm have a relative strong peak in the air-mass 1.5 global (AM1.5G) spectrum [10]; therefore, investigating the upconversion emission properties under the excitation of 1,540 nm may have a potential application value to reduce the solar cells' sub-bandgap losses and optical data storage, color display, infrared sensor and so on [11–17].

In this paper, the single-phase $BaSr_2Y_6O_{12}:Er^{3+}$ powders are prepared by solid-state reaction method for the first time, and the deep-ultraviolet upconversion emissions are detected under 1,540-nm excitation. Particularly, red emission combines downshifting with upconversion under 351- and 1,540-nm dual-wavelength excitation is also investigated. The properties of material combined downshifting with upconversion effect have been studied in the previous reports [18–20]. We discovered the synergistic effect between ultraviolet downconversion and infrared upconversion by employing the dual-wavelength (369 and 980 nm) excitation source. Further, in our work, the synergistic effect is also explored in $BaSr_2Y_6O_{12}:Er^{3+}$ powders using the 1,540-nm infrared and 351-nm ultraviolet dual wavelength as excitation source.

J. Zheng · X. F. Wang (✉) · W. Y. He · Y. Y. Bu · X. H. Yan
College of Electronic Science and Engineering,
Nanjing University of Posts and Telecommunications,
Nanjing 210046, China
e-mail: xfwang@njupt.edu.cn

X. H. Yan (✉)
College of Science, Nanjing University of Aeronautics and Astronautics, Nanjing 211106, China
e-mail: yanxh@njupt.edu.cn

2 Experimental

Powder samples of $BaSr_2Y_6O_{12}:Er^{3+}$ are synthesized via conventional high-temperature solid-state reaction in air. Analytical reagents BaO and SrO, high-purity Y_2O_3 (99.99 %) and Er_2O_3 (99.99 %) are used as raw materials. Each sample is weighed according to the nominal compositions $BaSr_2Y_{6(1-x)}O_{12}:6xEr^{3+}$($x = 0.02$, 0.04, 0.06, 0.08, 0.10, 0.15, 0.20) and then mixed thoroughly. The samples are filled in alumina crucibles and kept at 1,350 °C for 7 h in air atmosphere before decreasing temperature to ambient temperature.

The crystal structures of obtained samples are investigated by X-ray diffraction (XRD, Cu tube with Kα radiation at 1.54056 Å for $2\theta = 10-80°$). The Raman spectrum is measured by a laser micro-Raman spectrometer system. The excitation spectra and emission spectra of samples are measured by an Omni-λ3007 spectrophotometer with a photomultiplier tube with a CW Xe lamp (150 W) and a 1,540-nm variable power laser (0–150 mW) as the excitation light source. Among them, the 351-nm light source origin from a Xe lamp equipped with an optical grating monochromator. All the measurements are taken at room temperature.

3 Results and discussion

3.1 Sample synthesis

In our experiment, the $BaSr_2Y_6O_{12}$ powders with different Er^{3+} concentrations are obtained by simple solid-state method. Figure 1a shows the XRD patterns of $BaSr_2Y_{6(1-x)}O_{12}:6xEr^{3+}$ as a function of Er^{3+} concentration. The XRD patterns of $BaSr_2Y_{6(1-x)}O_{12}:6xEr^{3+}$ match well with the standard data in JCPDS Card file of NO. 72-0023, and the doping of Er^{3+} ions does not cause any significant change in the $BaSr_2Y_6O_{12}$ host structure. The Raman spectrum is excited by a 488-nm argon laser of $BaSr_2Y_6O_{12}$, which is shown in Fig. 1b. It is found that the spectrum shows several strong peaks corresponding to phonon modes with energy 217, 324, 379, 410 and 485 cm^{-1}. It is known that the host material with low phonon energies would have a high upconversion efficiency. The dependence of unit cell parameters a(Å), c(Å) and v(Å^3) on Er^{3+} concentration in $BaSr_2Y_{6(1-x)}O_{12}:6xEr^{3+}$ is shown in Fig. 2. The unit cell parameters a, c and v decrease linearly with the increasing Er^{3+} concentration, which accords with the Vegard's rule [21]. The linear decreasing trend of unit cell parameters is due to the substitution of Y^{3+} ions by small Er^{3+} ions in the host lattice. All these results indicate that the hexagonal phase $BaSr_2Y_6O_{12}$ is fully developed and a small amount of Er^{3+} ions successfully doped into the host.

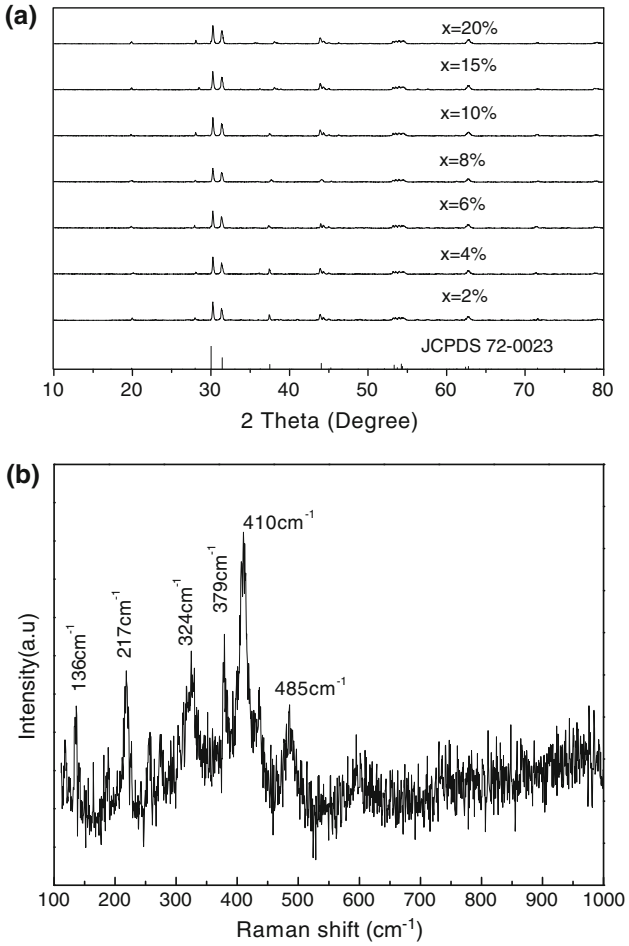

Fig. 1 **a** XRD pattern of as-prepared $BaSr_2Y_{6(1-x)}O_{12}:6xEr^{3+}$ ($x = 0.02$, 0.04, 0.06, 0.08, 0.10, 0.15, 0.20) and JCPDS Card (NO. 72-0023) of $BaSr_2Y_6O_{12}$. **b** The Raman spectrum of $BaSr_2Y_6O_{12}$

3.2 Photoluminescent properties

Figure 3 shows the upconversion emission spectra of $BaSr_2Y_{6(1-x)}O_{12}:6xEr^{3+}$ ($x = 0.02$) under 1,540-nm excitation. The ultraviolet and visible upconversion emissions are obtained. In particular, the ultraviolet emissions in the range of 260–350 nm are detected in these samples, as depicted in Fig. 3a. These emission peaks centered at 274, 297 and 324 nm come from the transitions of $^4G_{9/2}$, $^2K_{13/2}$ and $^2P_{3/2} \rightarrow {}^4I_{15/2}$ of Er^{3+} ions, respectively. All these ultraviolet emission peaks of Er^{3+} ions are rarely detected under the 1,540-nm excitation in the previous reports. In addition, it should also be noted that peaks centered at 382 and 408 nm are assigned to the $^4G_{11/2}$, $^2H_{9/2} \rightarrow {}^4I_{15/2}$ transition, as shown in Fig. 3b. Figure 3c depicts the upconversion emission spectrum in the range of 500–900 nm; these peaks are assigned to the following transitions: Near-infrared emission centered at 808 nm, red emission centered at 659 nm and green emission centered at 550 and 560 nm are assigned to the $^4I_{9/2} \rightarrow {}^4I_{15/2}$, $^4F_{9/2} \rightarrow {}^4I_{15/2}$ and $^2H_{11/2}$,

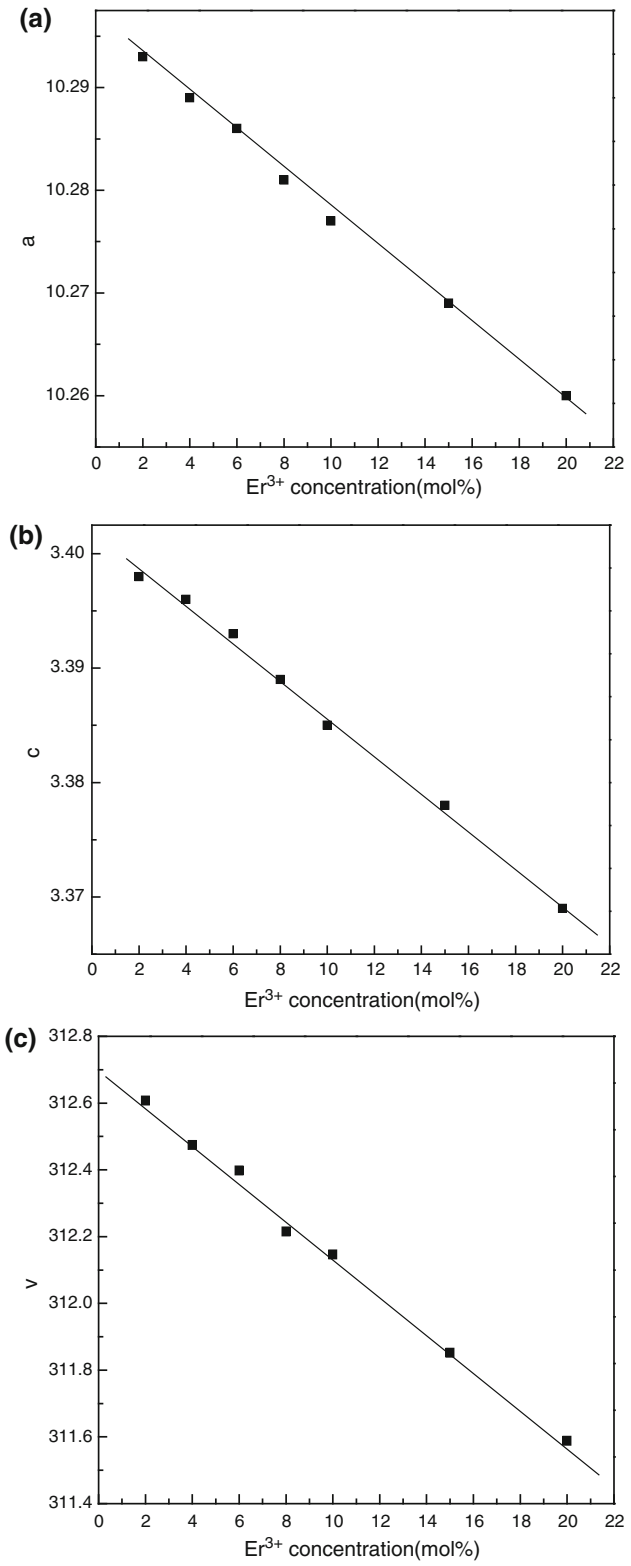

Fig. 2 Unit cell parameters a(Å), c(Å) and v(Å^3) dependence on Er^{3+} concentration in $BaSr_2Y_{6(1-x)}O_{12}$:6$x$$Er^{3+}$ (x = 0.02, 0.04, 0.06, 0.08, 0.10, 0.15, 0.20)

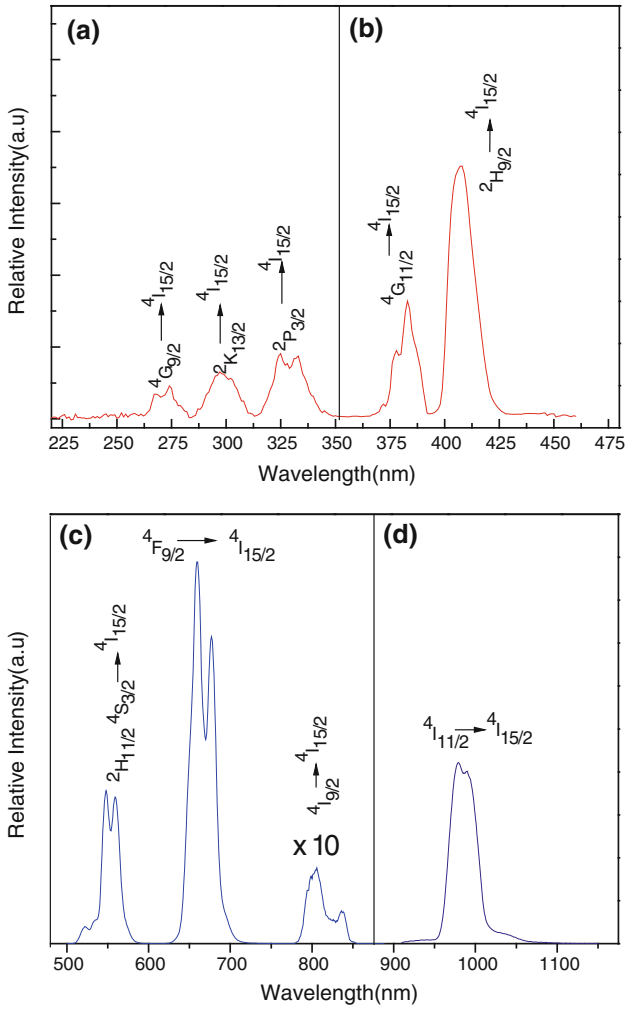

Fig. 3 UC luminescence spectrum of $BaSr_2Y_6O_{12}$:Er^{3+} (2 %) powder (λexc = 1,540 nm) in the range of **a** 250–350 nm, **b** 350–450 nm, **c** 500–800 nm and **d** 900–1,150 nm

$^4S_{3/2} \rightarrow {}^4I_{15/2}$ transitions of the Er^{3+} ions, respectively. Figure 3d gives the upconversion emission in the infrared region of 900–1,100 nm, the emission peak centered at 980 nm corresponding to the $^4I_{11/2} \rightarrow {}^4I_{15/2}$ of Er^{3+}. It should be pointed out that ultraviolet and blue emissions are measured with a higher voltage value of photomultiplier tube due to the weak emission (the same blow).

To investigate the contribution of Er^{3+} ions toward the photoluminescent (PL) properties of $BaSr_2Y_6O_{12}$:Er^{3+} powders, the emission intensities under 1,540-nm excitation are recorded for samples with different Er^{3+} ion concentrations, as shown in Fig. 4. The emission intensity is highly dependent on the Er^{3+} concentration. With the increasing Er^{3+} ion concentration, the intensity of all the emission regions increases firstly and reaches a maximum and then decreases remarkably when Er^{3+} concentration is

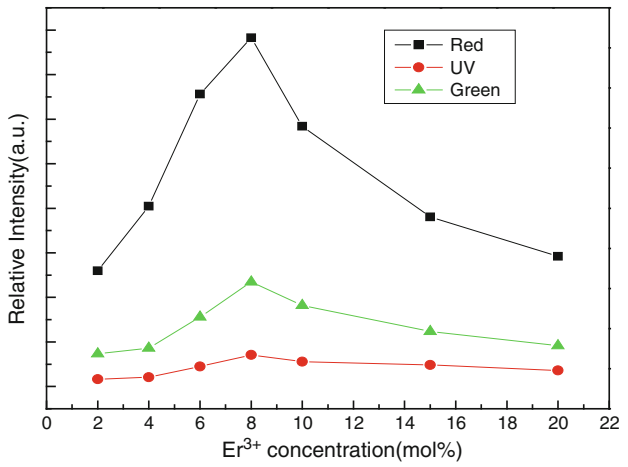

Fig. 4 The dependence of UC emission intensity at red, green and UV light on Er^{3+} doping concentration in $BaSr_2Y_{6(1-x)}O_{12}$:6xEr^{3+} ($x = 0.02, 0.04, 0.06, 0.08, 0.10, 0.15, 0.20$)

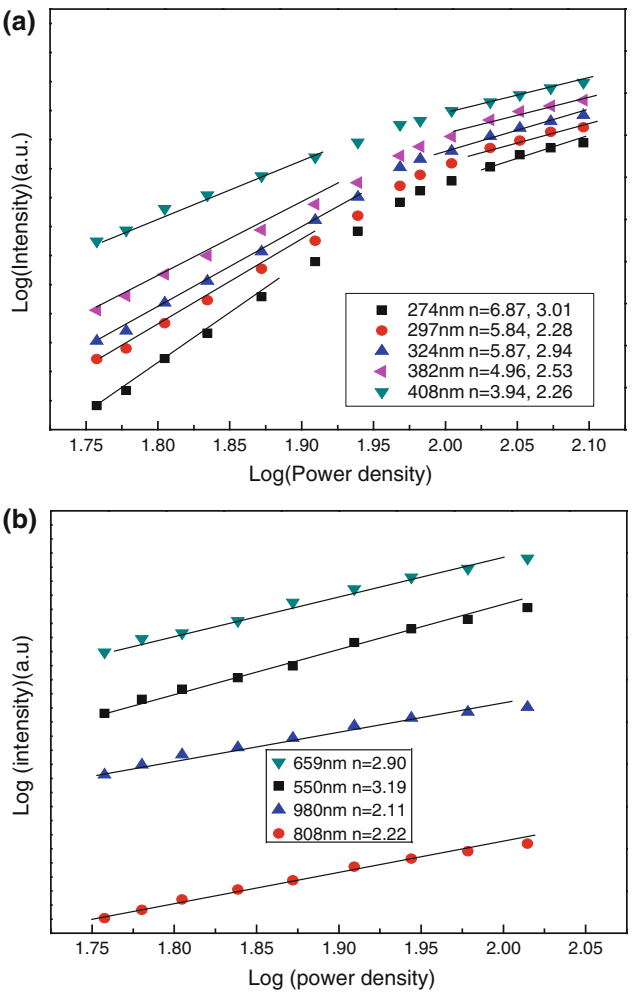

Fig. 5 Dependence of the upconversion emission intensity on excitation power density in $BaSr_2Y_6O_{12}:Er^{3+}$. **a** Ultraviolet and violet emission, **b** visible and infrared emission

further increased. This phenomenon is due to the Er^{3+} ions at high concentration that leads to the decrease in energy transfer effect, which is known as concentration quenching effect [22]. It is noted that the maximum emission intensity from all the regions of spectrum is observed for a critical concentration of 8 mol % Er^{3+}.

To better understand the physical mechanism responsible for the PL properties, the emission intensities are measured as a function of pumping power under 1,540-nm excitation. The upconverted emission intensity (I_{em}) depends on the pumping laser power density (P) according to the following equation [23]:

$$I_{em} \propto P^n, \quad (1)$$

where I_{em} is the fluorescence intensity, P is the pumping power density of the 1,540-nm laser, the power density is calculated from the ratio between the laser power and the area of light spot, and n is the number of pumping photons absorbed per upconverted photon emitted. Figure 5 shows the logarithmic plot of the integrated emission intensities of the upconverted emission bands in the region of ultraviolet light, violet, green and red as a function of the pumping laser power density. The output slopes (n) for ultraviolet and violet upconversion emissions centered at 274, 297, 324, 382 and 408 nm are 6.87, 5.84, 5.87, 4.96 and 3.94, respectively, indicating that seven-, six-, six-, five- and four-photon processes are responsible for the populating of $^2P_{3/2}$, $^4G_{11/2}$, $^2K_{13/2}$, $^4G_{9/2}$ and $^2H_{9/2}$, states of Er^{3+} ions. When the power density increases to about 90 mW/mm^2, the output slope (n) of log-log graph is out of shape, and the corresponding slopes of linear fittings are reduced to 3.01, 2.28, 2.94, 2.53 and 2.26 for 274, 297, 324, 382 and 408 nm, respectively. The numbers of photons decrease rapidly when the excitation power exceeds digital, owing to the competition between the linear decay and the upconversion processes for the depletion of the intermediate excited states [24]. In addition, the n values for red and green emission bands are all around 3, indicating that populating the $^2H_{11/2}$, $^4S_{3/2}$ and $^4F_{9/2}$ levels needs three 1,540-nm photons and is a three-photon process. For the emission peaked at 808 and 980 nm, the n value is 2.22 and 2.11, respectively, indicating two-photon process.

The photoluminescence excitation spectrum (PLE) of Er^{3+}: $^4F_{9/2} \rightarrow {}^4I_{15/2}$ emission (659 nm) is shown in Fig. 6a, in which an excitation peak in UV region centered at 351 nm is observed, which corresponds to the $^4I_{15/2} \rightarrow {}^2G_{7/2}$ transition of Er^{3+} ion. Figure 6b shows the downshifting emission spectrum of sample under 351-nm excitation, the red region emission centered at 659 nm is assigned to the transition of $^4F_{9/2} \rightarrow {}^4I_{15/2}$ of Er^{3+} ion, and the infrared characteristic emissions of Er^{3+} from $^4I_{11/2}$ (980 nm) and $^4I_{13/2}$ (1,540 nm) levels are presented here clearly. The insert of Fig. 6 shows the dependence of red

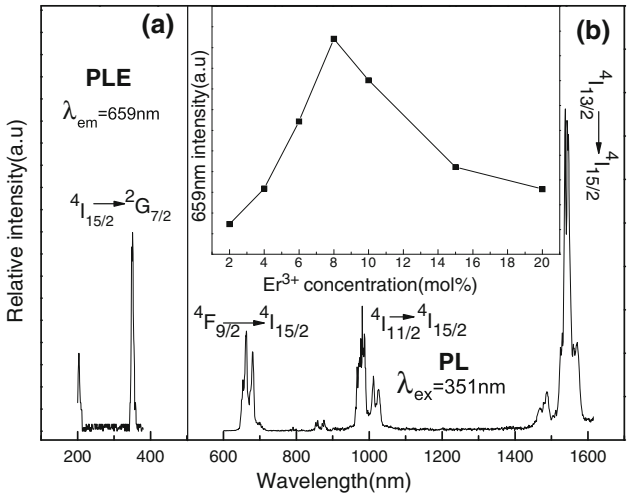

Fig. 6 **a** The PLE spectra of Er^{3+}: $^4F_{9/2} \rightarrow {}^4I_{15/2}$ emission (659 nm) in $BaSr_2Y_6O_{12}$:2 %Er^{3+}. **b** The visible and infrared photoluminescent spectrum of sample under 351-nm excitation. The *inset* shows the dependence of red emission intensity on Er^{3+} ions doping concentration under 351-nm excitation in $BaSr_2Y_{6(1-x)}O_{12}$:6xEr^{3+} ($x = 0.02$, 0.04, 0.06, 0.08, 0.10, 0.15, 0.20)

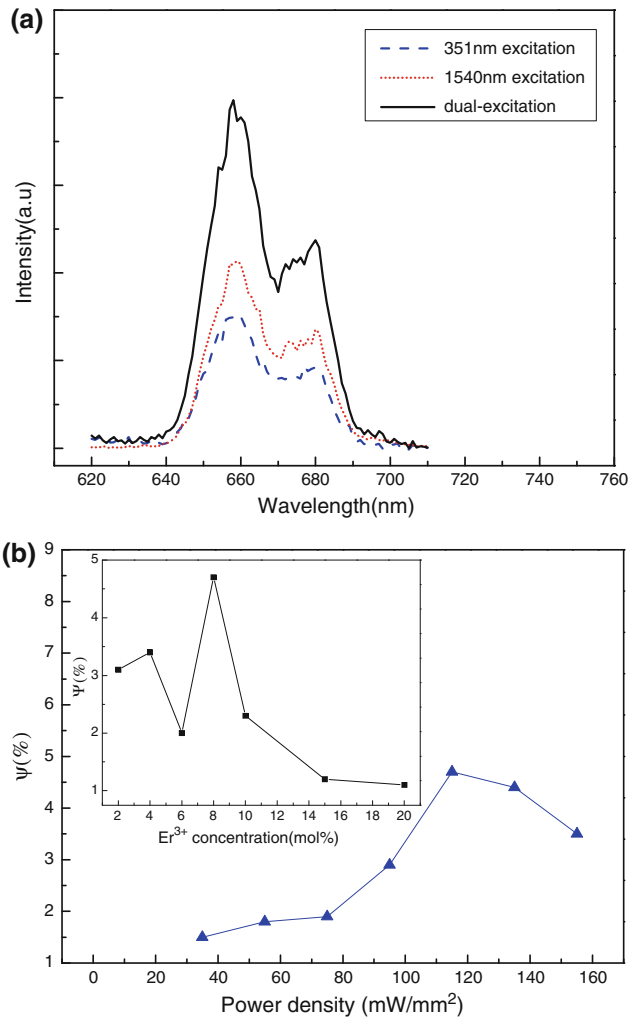

Fig. 7 **a** The red emission spectra of $BaSr_2Y_6O_{12}$:Er^{3+} under 351-nm excitation, under 1,540-nm excitation and under 1,540- and 351-nm dual excitation. **b** The dependence of absolute enhancement rate (ψ) of red emission on Er^{3+} concentration in $BaSr_2Y_{6(1-x)}O_{12}$:6xEr^{3+} ($x = 0.02$, 0.04, 0.06, 0.08, 0.10, 0.15, 0.20), on 1,540-nm laser power density when 351-nm power density fixed at 0.8 mW/mm^2 (the *inset*)

emission intensities on Er^{3+} doping concentration under the excitation of 351 nm. It is noticed that the emission intensity of red emission increases rapidly with the increasing Er^{3+} doping concentration; however, a decreasing trend is observed clearly when concentration is set to more than 8 mol % due to concentration quenching.

As described above, the emission band of Er^{3+} ions centered at 659 nm is observed under 1,540- and 351-nm single excitation, respectively. However, under the 1,540- and 351-nm dual excitation, a synergistic effect is witnessed in these samples, which shows that the red emission intensity under the 1,540-nm and 351-nm dual excitation is stronger than the sum of red emission intensity under the 351- and 1,540-nm single excitation. To quantitatively describe the synergistic effect, the absolute enhancement rate (ψ) of red emission can be defined as follows [20]:

$$\psi = \frac{I_3 - (I_1 + I_2)}{I_1 + I_2}, \quad (2)$$

where I_1, I_2 and I_3 are the integrated intensity of red emission bands under 1,540-nm excitation, under 351-nm excitation and under 1,540- and 351-nm dual excitation, respectively. The red emission bands, the dependence of red emission absolute enhancement rate on 1,540-nm power density and Er^{3+} doping concentration are shown in Fig. 7a, b and inset, respectively. When the maximum value ($\psi = 4.7$ %) is witnessed, the excitation power density of 1,540-nm semiconductor laser is adjusted to 115 mW/mm^2 and the excitation power density of 351 nm is fixed at 0.8 mW/mm^2 in 8 mol %Er^{3+}-doped $BaSr_2Y_6O_{12}$ sample.

3.3 Upconversion process and synergistic effect mechanism

It is no doubt that ET, excited/ground-state absorption (ESA/GSA) and non-radiative relaxation (NR) processes can be accounted for the upconversion emission mechanisms in $BaSr_2Y_6O_{12}$:Er^{3+} under the excitation of 1,540-nm semiconductor laser [25, 26]. The possible upconversion procedure is schematically illustrated in Fig. 8. As to the ultraviolet emission, for populating $^2K_{13/2}$ and $^4G_{9/2}$ levels as examples, a possible upconversion process is provided as follows:

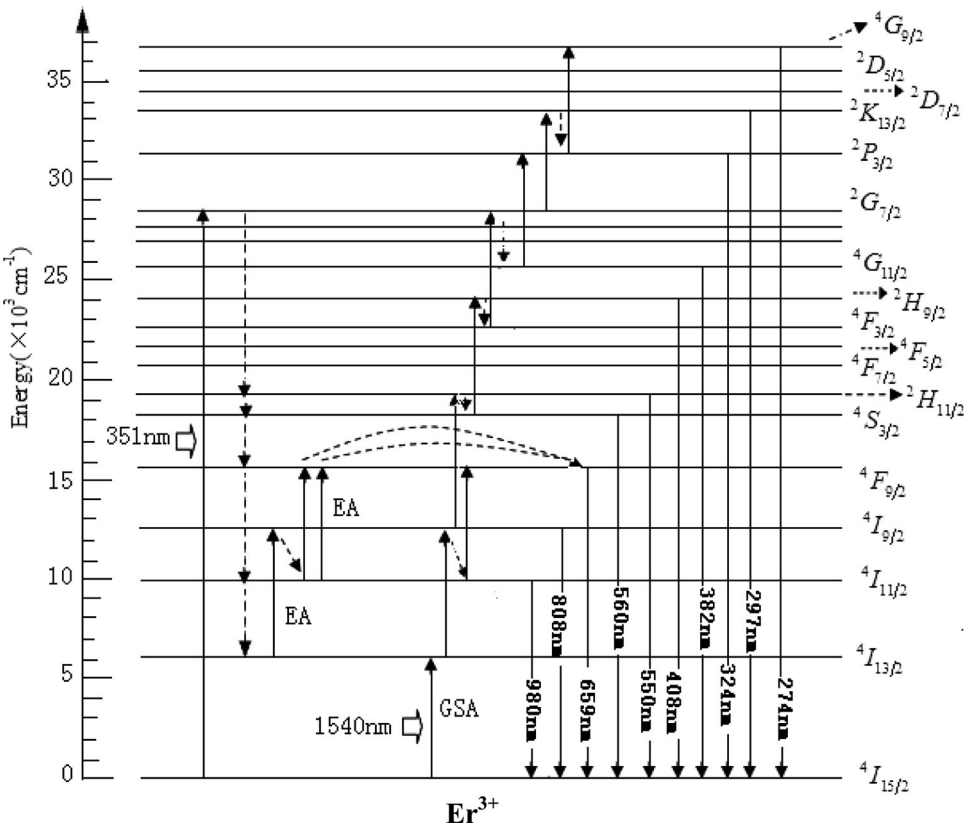

Fig. 8 Energy-level diagram of Er^{3+}, upconversion and downshifting process under excitation of 1,540 and 351 nm, respectively, and the possible mechanism of synergistic effect for red emission under the 351- and 1,540-nm dual excitation

$$^4I_{15/2} \xrightarrow{GSA} {}^4I_{13/2} \xrightarrow{ESA/ET} {}^4I_{9/2} \xrightarrow{ESA/ET} {}^2H_{11/2} \xrightarrow{NR} {}^2S_{3/2} \xrightarrow{ESA/ET} {}^2H_{9/2} \xrightarrow{NR} {}^4F_{3/2} \xrightarrow{ESA/ET} {}^2G_{7/2} \xrightarrow{ESA/ET} {}^2K_{13/2} \xrightarrow{NR} {}^2P_{3/2} \xrightarrow{ESA/ET} {}^4G_{9/2}.$$

Populating $^2K_{13/2}$ and $^4G_{9/2}$ are assigned to six- and seven-photon upconversion processes, respectively, as the above process, which accords with the calculated n as shown in Fig. 5a.

The mechanism resulting in upconversion emission occurs via two distinct processes acting concomitantly: ESA and ET processes. It is well known that both processes are dependent upon doping concentration. While the ET rate is stronger depending on the distance between the ions involved than the ESA process, and once over a critical distance, the efficiency of energy transfer mechanism will be decreased rapidly [27]. The different slopes of intensity in different regions of emission are observed with the increasing concentration as shown in Fig. 4; the slope of red emission is greater than the others; we deduce that ET process is the dominant mechanism for populating the low energy levels, while the ESA process becomes the dominant mechanism, which is responsible for populating the high energy level of Er^{3+}.

In addition, the possible mechanism of synergistic effect is also proposed, as shown in Fig. 8. Under the 1,540-nm excitation, the Er^{3+} ions are excited to the $^4I_{9/2}$ level through successively absorbing two 1,540-nm photons, some of Er^{3+} ions at $^4I_{9/2}$ level into the $^4I_{11/2}$ level through a non-radiative relaxation process. Then, the cross-relaxation process from $Er^{3+}(^4I_{13/2})$ to $Er^{3+}(^4I_{11/2})$ and ESA process occur simultaneously: $Er^{3+}(^4I_{13/2} \rightarrow {}^4I_{15/2})$, $Er^{3+}(^4I_{11/2} \rightarrow {}^4F_{9/2})$, which leads to the red upconversion emission ($^4F_{9/2} \rightarrow {}^4I_{15/2}$). Under the 351-nm excitation, $^2G_{7/2}$ level of Er^{3+} ion is populated through GSA process, and then the red luminescent centered at 659 nm due to a NR process from $^2G_{7/2}$ to $^4F_{9/2}$ [28, 29]. Besides, the $^4I_{11/2}$ and $^4I_{13/2}$ levels are also populated through non-radiative relaxation process in downshifting process. In general, some of the energy in the $^4I_{11/2}$ and $^4I_{13/2}$ levels of Er^{3+} ions is dissipated via thermal energy; however, under the 351- and 1,540-nm dual excitation, the Er^{3+} ions in the $^4I_{11/2}$ and $^4I_{13/2}$ levels from NR process can be excited again (EA) to the $^4F_{9/2}$ level by absorbing 1,540-nm photons as follows:

$$^4I_{15/2} \xrightarrow{GSA} {}^2G_{7/2} \xrightarrow{NR} {}^4I_{11/2} \xrightarrow{EA} {}^4F_{9/2} \xleftarrow{EA} {}^4I_{11/2} \xleftarrow{NR} {}^4I_{9/2} \xleftarrow{EA} {}^4I_{13/2} \xleftarrow{NR} {}^2G_{7/2} \xleftarrow{GSA} {}^4I_{15/2}.$$

Therefore, the energy of non-radiative relaxation is excited again, resulting in the synergistic enhancement effect of red emission ($^4F_{9/2} \rightarrow {}^4I_{15/2}$) under the dual excitation.

4 Conclusion

In summary, the preparation and photoluminescence properties of single-phase $BaSr_2Y_6O_{12}:Er^{3+}$ are investigated systemically for the first time. Power-dependent studies reveal that ultraviolet emissions of Er^{3+} under 1,540-nm excitation result from a seven-, six- and five-photon process, and the ultraviolet upconversion mechanism is discussed based on complex ESA and GSA/ESA processes. Additionally, a synergistic effect combined ultraviolet downshifting with infrared upconversion, which shows that the red emission intensity under the 1,540- and 351-nm dual excitation is stronger than the sum of red emission intensities under the 351- and 1,540-nm single excitation, and the maximum absolute enhancement rate is 4.7 %. It is believed that the $^4I_{13/2}$ and $^4I_{11/2}$ levels of Er^{3+} from non-radiative relaxation process under 351-nm excitation are excited again to $^4F_{9/2}$ level by absorbing 1,540-nm infrared photon in the 351- and 1,540-nm dual-excitation process, which is responsible for the synergistic effect of red emission.

Acknowledgments This work was supported financially by National Natural Science Foundation of China (No. NSFC51032002), the key Project of the National High Technology Research and Development Program ("863" Program) of China (No. 2011AA050526) and the Science and Technology Support Plan of Jiangsu Province (BE2011191), Natural Science Youth Foundation of Jiangsu Province (BK20130865).

References

1. X.S. Wang, J. Song, H.Y. Sun, Z.Z. Xu, J.R. Qiu, Opt. Express **15**, 1384 (2007)
2. X.F. Wang, X.H. Yan, C.X. Kan, J. Lumin. **131**, 2325 (2011)
3. Q.J. Chen, W.J. Zhang, X.Y. Huang, G.P. Dong, M.Y. Peng, J. Alloy Compd. **513**, 1814 (2012)
4. Y.Y. Zhang, L.W. Yang, C.F. Xu, J.X. Zhong, C.Q. Sun, Appl. Phys. B **98**, 243 (2010)
5. D.Q. Chen, Y.S. Wang, Y.L. Yu, J. Rare Earth. **26**, 428 (2008)
6. C.Y. Cao, W.P. Qin, J.S. Zhang, Opt. Lett. **33**, 857 (2008)
7. F. Qin, Y.D. Zheng, Y. Yu, C.B. Zheng, P.S. Tayebi, Opt. Commun. **284**, 3114 (2011)
8. K.Z. Zheng, D. Zhao, D.S. Zhang, N. Liu, W.P. Qin, Opt. Lett. **35**, 2442 (2010)
9. K.Z. Zheng, Z.Y. Liu, D. Zhao, D.S. Zhang, G.S. Qin, W.P. Qin, Opt. Mater. **33**, 783 (2011)
10. S.K.W. MacDougall, I. Aruna, J. Marques-Hueso, K.W. Krämer, B.S. Richards, Opt. Express **15**, A879 (2012)
11. M. Yan, V.D. Ende, L. Aarts, A. Meijerink, Phys. Chem. **11**, 11081 (2009)
12. V.K. Tikhomirov, V.D. Rodriguez, J. Méndez-Ramos, J. Castillo, D. Krilenko, G. Van Tendeloo, V.V. Moshchalkov, Sol. Energ. Mat. Sol. C **100**, 209 (2012)
13. A. Shalav, B.S. Richards, M.A. Green, Sol. Energ. Mat. Sol. C **91**, 829 (2007)
14. T. Trupke, A. Shalav, B.S. Richards, P. Würfel, M.A. Green, Sol. Energ. Mat. Sol. C. **90**, 3327 (2006)
15. K. Deng, T. Gong, L.X. Hu, X.T. Wei, Y.H. Chen, Opt. Express **19**, 1749 (2011)
16. D. Mihailovic, D. Dvorsek, V.V. Kabanov, J. Demsar, L. Forro, H. Berger, Appl. Phys. Lett. **80**, 871 (2002)
17. E. Downing, L. Hesselink, J. Ralston, R. Macfarlane, Science **273**, 1185 (1996)
18. H. Lin, J. Marqués-Hueso, D.Q. Chen, Y.S. Wang, B.S. Richards, Mater. Res. Bull. **47**, 4433 (2012)
19. Q.J. Chen, W.J. Zhang, X.Y. Huang, G.P. Dong, M.Y. Peng, Q.Y. Zhang, J. Alloy. Compd. **513**, 139 (2012)
20. X.F. Wang, X.H. Yan, Opt. Lett. **36**, 4353 (2011)
21. L. Vegard, Z. Angew. Phys. **5**, 17 (1921)
22. G. Blasse, Phys. Lett. A. **28**, 444 (1968)
23. M. Pollnau, D.R. Gamelin, S.R. Lüthi, H.U. Güdel, Phys. Rev. B. **61**, 3337 (2000)
24. Y.Q. Lei, H.W. Song, L.M. Yang, L.X. Yu, Z.X. Liu, G.H. Pan, X. Bai, L.B. Fan, J. Chem. Phys. **123**, 174710 (2005)
25. P. Ghosh, S. Sadhu, T. Sen, A. Patra, Bull. Mater. Sci. **31**, 461 (2008)
26. H. Guo, M. Yin, W.P. Zhang, J. Rare Earth. **24**, 740 (2006)
27. J.A. Capobianco, F. Vetrone, J.C. Boyer, J. Phys. Chem. B **106**, 1181 (2002)
28. L. Aarts, B.M. van der Ende, A. Meijerink, J. Appl. Phys. **106**, 23522 (2009)
29. R. Mupparapu, K. Vynck, I. Malfanti, S. Vignolini, M. Burresi, P. Scudo, R. Fusco, D.S. Wiersma, Opt. Lett. **37**, 368 (2012)